Proceedings of Engineering & Technology -PET Vol 96, pp.95-103 **Advances in Energy Transition and Environmental Impacts**

Unsteady Forced Convection Analysis in a Straight Channel with a Rough Porous Obstacle and a Rigid Baffle

Khaoula Dehdouh[1], Brahim Fersadou[2], Henda Kahalerras [3], Lakhdari Yahia Abdelhamid [4]

[1,2,3,4] *Department of Mechanical and Process Engineering, University of Sciences and Technology Houari Boumediene (USTHB), Algeria.*

kdehdouh@usthb.dz[1]; brahim.fersadou@usthb.edu.dz[2]; henda.kahalerras@usthb.edu.dz[3]; y.lakhdari@hotmail.com[4]

***Abstract*—This numerical study focuses on unsteady two-dimensional forced convection in a straight channel equipped with a baffle dividing the space into two compartments with differential heating. Each compartment is subjected to thermal sources maintained at uniform temperatures. The first compartment contains a porous obstacle made of metallic foam, whose outer surface may be either smooth or rough. A water-based nanofluid with carbon nanotubes flows through the channel at a velocity corresponding to a laminar regime, with a uniform inlet temperature. The governing equations were solved using the finite element method. The nanofluid flow through the porous obstacle is modeled using the generalized Darcy–Brinkman–Forchheimer model. The studied parameters include: the height of the baffle (0 cm ≤ H_b ≤ 0.75 cm); the properties of the porous obstacle: porosity (ε, 0.8 ≤ ε ≤ 0.98), pore density (20 PPI ≤ ω ≤ 50 PPI), roughness amplitude (0.1 cm ≤ A ≤ 0.2 cm), and number of roughness elements (4 ≤ N ≤ 10). The results show a significant enhancement in heat transfer due to the integration of the porous obstacle and the baffle. Specifically, a porous obstacle with high pore density improves heat transfer in the first compartment, while a tall baffle promotes thermal performance in the second compartment. An in-depth analysis identified the optimal configurations that ensure efficient heat transfer throughout the system while minimizing pressure drop.**

Keyword: **Straight channel; Porous obstacle; Rough obstacle; Forced convection; Metal foam; Nanofluid; Rigid baffle.**

I. INTRODUCTION:

The demand for performance and miniaturization of technological devices has driven the development of cooling techniques, particularly nanofluids and passive methods. Efficient heat dissipation is crucial to prevent system degradation. Several numerical studies illustrate these advances.

Research on flow around cylinders, such as that by Amrit Pal Singh Bhinder et al. [1], shows the correlation between vortex structures and heat transfer. While nanofluids enhance thermal conductivity, they pose the challenge of accurately predicting their properties. R. Deepak Selvakumar et al. [2] compared different methods to characterize a TiO_2-based nanofluid, confirming its potential but noting discrepancies between models.

The addition of magnetic fields amplifies these effects. Fatih Selimefendigil et al. [3] and Nikelham et al. [4] demonstrate that a magnetic field combined with nanoparticles (CuO, Al_2O_3) significantly improves heat transfer and alters the flow.

The optimization of passive configurations is also explored. The work of Dalei Jing et al. [5] and Abdolrahman Dadvand et al. [6] on microchannels equipped with flexible turbulators and obstacles shows substantial gains in thermal performance and mixing.

Finally, fundamental studies on non-Newtonian fluids (Huahai Zhang et al. [7]) and porous media (Shohre Heydari et al. [8]) reveal complex behaviors influencing heat transfer.

In this context, the present study introduces an innovation for passive cooling of power electronics: the insertion of a rough-surfaced porous obstacle into a channel with heat sources and a rigid turbulator, using

ISSN: 1737-9334

a carbon nanotube-based nanofluid. The objective is to evaluate hydrothermal performance by varying several geometric and physical parameters.

II. MATHEMATICAL FORMULATION:

II.1. Physical Domain

The physical domain under study is a channel with a length of 10 cm and a height of 1 cm. The lower wall features, at its midpoint, a rigid baffle of height H_b and negligible width. The lower wall also includes two cold sources maintained at a temperature T_c = 25 °C, while the upper wall contains two hot sources maintained at T_h = 90 °C. A circular metal foam obstacle, with a diameter D = 0.32 cm, is placed at the center of the channel at x_1 = 1.5 cm from the inlet.
A nanofluid enters the channel with an inlet velocity U_i = 0.1343 m/s (corresponding to a Reynolds number Re = 1500) and an inlet temperature T_i = 25 °C.

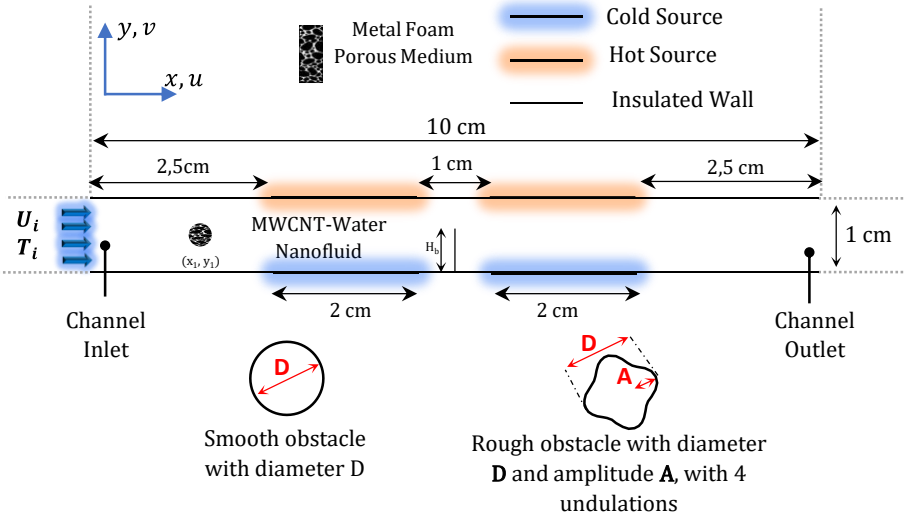

Fig. 1: Physical domain

II.2. Hypothesis

The resolution of the complex phenomena present in our study requires some simplifying assumptions. The flow is considered two-dimensional, in an unsteady and laminar regime. The base fluid is incompressible and Newtonian, and viscous dissipation as well as any internal heat source are neglected. The nanofluid is treated as a homogeneous mixture, where the nanoparticles and the base fluid are in local thermal equilibrium. The buoyancy force is considered negligible. The porous medium, made of a metal foam, is isotropic, homogeneous, and saturated by the nanofluid, which is in local thermal equilibrium with the solid matrix. Finally, the nanoparticles, which are smaller than the porous matrix, are kept suspended in the base fluid using surfactants, which prevents their agglomeration and deposition on the solid matrix.
Continuity equation

II.3. Governing equations

The governing equations were formulated using the homogeneous flow approach for the nanofluid and the Darcy-Brinkman-Forchheimer model to describe the flow through the metallic foam porous obstacle.

$$\frac{\partial u}{\partial x}+\frac{\partial v}{\partial y}=0 \quad (1)$$

ISSN: 1737-9334

Proceedings of Engineering & Technology -PET Vol 96, pp.95-103 **Advances in Energy Transition and Environmental Impacts**

Navier–Stokes equations:

-according to X:

$$\frac{\rho_{nf}}{\delta_3 \varepsilon}\frac{\partial u}{\partial t}+\frac{\rho_{nf}}{\delta_1 \varepsilon^2}\left(u\frac{\partial u}{\partial x}+v\frac{\partial u}{\partial y}\right)=-\frac{\partial p}{\partial x}+\mu_{eff}\left(\frac{\partial^2 u}{\partial x^2}+\frac{\partial^2 u}{\partial y^2}\right)-\frac{\mu_{nf}}{K}u\delta_2-\frac{\rho_{nf}\,C}{\sqrt{K}}|\vec{V}|u\delta_2 \quad (2)$$

-according to Y:

$$\frac{\rho_{nf}}{\delta_3 \varepsilon}\frac{\partial v}{\partial t}+\frac{\rho_{nf}}{\delta_1 \varepsilon^2}\left(u\frac{\partial v}{\partial x}+v\frac{\partial v}{\partial y}\right)=-\frac{\partial p}{\partial y}+\mu_{eff}\left(\frac{\partial^2 v}{\partial x^2}+\frac{\partial^2 v}{\partial y^2}\right)-\frac{\mu_{nf}}{K}v\delta_2-\frac{\rho_{nf}\,C}{\sqrt{K}}|\vec{V}|v\delta_2 \quad (3)$$

Energy equation :

$$(\rho C_p)_{eff}\frac{\partial T}{\partial t}+(\rho C_p)_{nf}\left(u\frac{\partial T}{\partial x}+v\frac{\partial T}{\partial y}\right)=k_{eff}\left(\frac{\partial^2 T}{\partial x^2}+\frac{\partial^2 T}{\partial y^2}\right) \quad (4)$$

We take the constants $\delta_1=\delta_2=1$, in the porous obstacle region.

In the nanofluid region, we take $\delta_1=\frac{1}{\varepsilon^2}\ et\ \delta_2=0$ as well as $\mu_{eff}=\mu_{nf}$ and $k_{eff}=k_{nf}$

II.4. Boundary conditions

The boundary conditions related to the above equations are:

At the inlet: $u=U_i\,;v=0;\ T=T_i$ (5)

At the top wall:
$$\begin{cases} u=v=0;\ T=T_h & hot\ ribbon \\ u=v=\frac{\partial T}{\partial y}=0 & elsewhere \end{cases} \quad (6)$$

At the bottom wall:
$$\begin{cases} u=v=0;\ T=T_c & colde\ ribbon \\ u=v=\frac{\partial T}{\partial y}=0 & elsewhere \end{cases} \quad (7)$$

At the outlet: $\frac{\partial u}{\partial x}=v=\frac{\partial T}{\partial x}=0$ (8)

II.5. nanofluid and metal foam properties

For the water/MWCNT nanofluid, the thermophysical properties and their correlations are derived from the model of [9], except for the viscosity, which is taken from the study of [10]. For the metal foam, the characteristics are sourced from the study of [11], except for the effective conductivity, which is modeled according to [12].

II.6. Nusselt numbers and pressure drop

Heat transfer is represented by the local Nusselt number, defined as:

$$Nu_i=\frac{h\,H}{k_{nf}} \quad (9)$$

i=1 for the first heat source located upstream of the baffle

i=2 for the second heat source located downstream of the baffle

Whereas the average Nusselt number is determined by the following expression:

$$Nu_{mi}=\frac{1}{s}\int_{x=2,5\ cm-5,5\ cm}^{x=4,5\ cm-7,5\ cm} Nu\ dx \quad (10)$$

The average Nusselt number for the two hot sources is defined by:

$$Nu_m=(Nu_{m1}+Nu_{m2})/2 \quad (11)$$

The time-averaged overall Nusselt number is expressed as follows:

$$Nu_g=\frac{1}{t}\int_{t=0\ s}^{t=8\ s} Nu_m\ dt \quad (12)$$

The pressure drop between the inlet and the outlet of the cavity is given by:

$$\Delta P=P_m(x=0\ cm)-P_m(x=10\ cm) \quad (13)$$

$$P_m=\int_{y=0\ cm}^{y=1\ cm} P\,dy \quad (14)$$

ISSN: 1737-9334

Proceedings of Engineering & Technology -PET Vol 96, pp.95-103 **Advances in Energy Transition and Environmental Impacts**

The time-averaged pressure drop is given by:

$$\Delta P_g = \frac{1}{t} \int_{t=0\ s}^{t=6\ s} \Delta P \ dt \tag{15}$$

A performance factor is used to compare the heat transfer enhancement to the pressure drop losses. It is defined as:

$$PEC = \frac{{Nu_m}/{(Nu_m)_{ref}}}{\left({\Delta P}/{\Delta P_{ref}}\right)^{1/3}} \tag{16}$$

The reference case is a system with a smooth obstacle for the same densities and a baffle with H_b = 0.5 cm.

III. NUMERICAL PROCEDURE

The coupled heat transfer and fluid flow equations were solved using the finite element method, which is suited to the complex geometries and boundary conditions of the study. The system of discretized equations was solved via the GMRES method with preconditioning, applying a strict convergence criterion of 10^{-6}. A mesh sensitivity study confirmed result independence from 49,060 elements onward, with an average element quality of approximately 0.86. A time step of $\Delta t = 10^{-2}$ was selected.

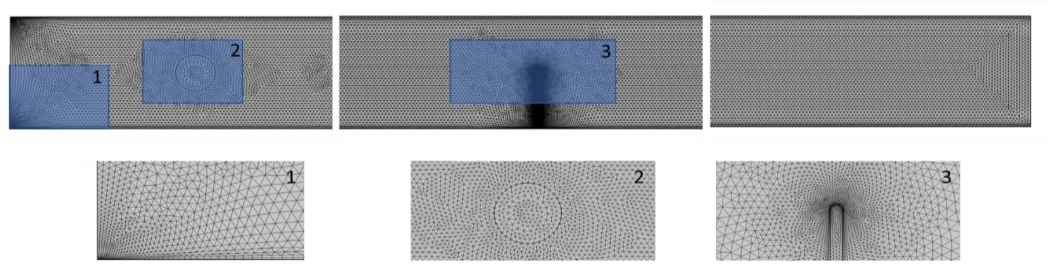

Fig 2: Unstructured mesh with 49060 elements.

The accuracy of the computational code developed for this work is confirmed by comparing its results with the values reported by Sajjad et al. [13], who analyzed the impact of adding straight fins on the thermal and hydraulic performance of transient forced convection flow around a circular cylinder. The results in Table 3 reveal a maximum deviation of 0.83%.

Table 3: The variation of averaged Nusselt number with respect to the number of fins attached to cylinder with non-dimensional height of 0.35 at different Reynolds numbers.

	Re=100			Re=200		
Fin number	Sajjad et al.[13]	Present study	Relative error	Sajjad et al.[13]	Present study	Relative error
0	5,80	5,84	0,60	8,56	8,63	0,81
4	4,21	4,24	0,58	6,73	6,79	0,79
10	2,44	2,45	0,50	3,62	3,65	0,73

IV. RESULTS AND DISCUSSION

In the present work, several parameters were studied to examine their impact on the system's hydrothermal performance. To simplify the study, some control parameters were fixed while others were varied. Specifically, the channel length was set to L = 10 cm and the height to H = 1 cm. The nanoparticle

ISSN: 1737-9334

volume fraction was $\phi = 0.3\%$. The nanofluid enters the channel with an inlet velocity Ui = 0.1343 m/s and temperature T_i = 25 °C. The hot sources are maintained at Tc = 90 °C and the cold sources at $T_c = T_i$. Additionally, the following parameters were varied: the rigid baffle height (Hb) (0 cm ≤ H_b ≤ 0.75 cm), the porosity of the porous block ($0.8 \leq \varepsilon \leq 0.98$), the pore density ($20 \leq \omega \leq 50$), the amplitude of the corrugations forming the porous block roughness (A = 0.01 cm and A = 0.02 cm), and the number of corrugations in the porous block ($4 \leq N \leq 10$).

a. Effect of the rigid baffle height H_b:

In this section, we analyze the effect of the height of a rigid baffle (H_b) on a nanofluid flow around a smooth circular porous obstacle (50 PPI, ε=0.8). Simulations over 6 seconds reveal the periodic formation of Von Kármán vortices starting at t=2 s, influencing the velocity, pressure, and temperature fields.
Adding a baffle downstream modulates these vortices. For a low baffle (H_b = 0.25 cm), the initial vortex structures are slightly attenuated with limited impact on the flow and thermal fields. When the baffle height is increased to Hb = 0.5 cm, the structure of the Von Kármán vortices is altered, leading to increased recirculation, and enhanced thermal mixing due to the interaction between primary and secondary vortices. A high baffle (H_b = 0.75 cm) significantly disrupts the initial vortex system, replacing it with a complex pattern of interacting vortices. This results in strong lateral acceleration, intense low-pressure zones downstream, and optimal heat transfer due to superior fluid mixing.
Upstream, the flow through the aluminum foam porous matrix is predominantly hindered by inertial losses (Darcy-Forchheimer effects). Overall, the baffle acts as a vortex modulator, capable of enhancing the system's thermal performance, particularly at greater heights.

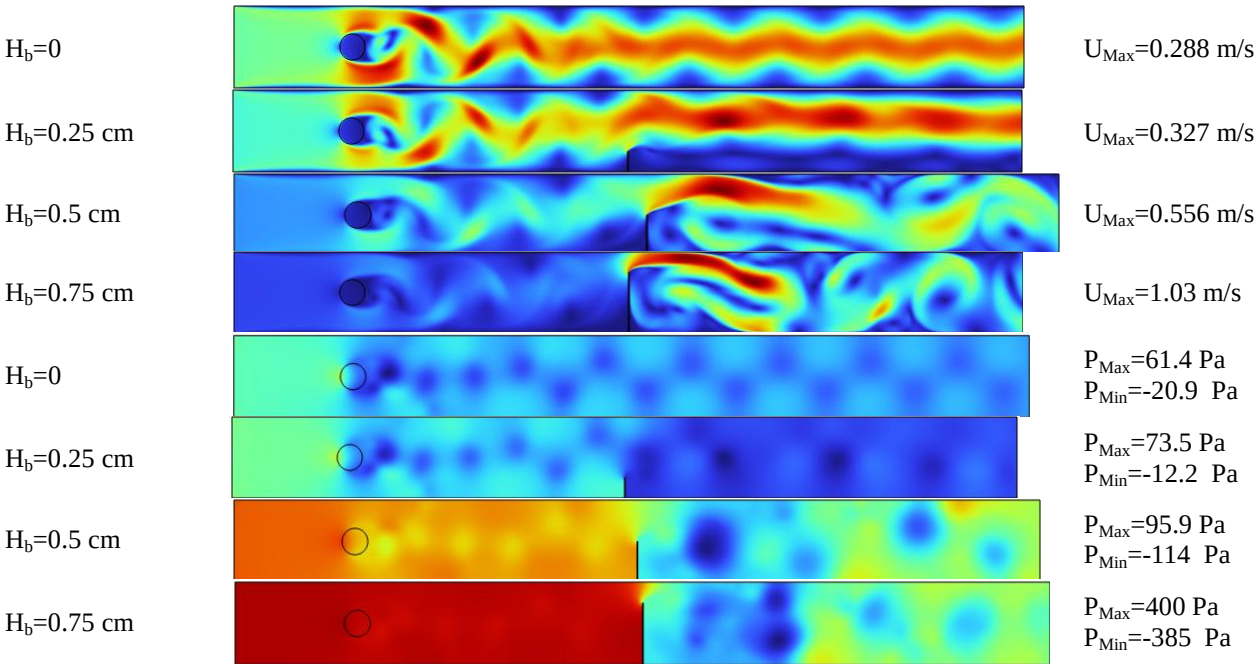

Fig 3: Velocity contours and pressure contours at 6 seconds for different baffle heights; smooth porous obstacle, ε=0.8 and ω=50 PPI.

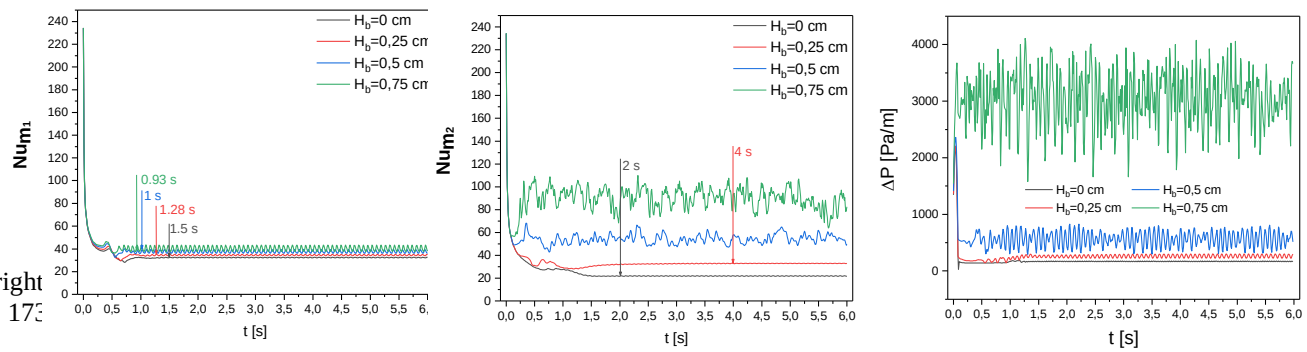

Fig 4: Temporal evolution of the average Nusselt number of the hot sources and the pressure drop for different baffle heights,

For Figure 4, we observe that a high baffle (Hb = 0.75 cm) significantly improves heat transfer and accelerates the establishment of the periodic regime linked to Von Karman vortices. For the second source, the improvement is confirmed, but the complex interaction of the downstream vortices delays this periodic regime. At maximum Hb, perturbations amplify and lead to a chaotic regime, demonstrating the dominant influence of vortices on heat transfer.High baffles generate significantly greater pressure drops, which is confirmed by the pressure contours in Figure 3 showing a stronger gradient and more distorted isobars.

b. Effect of the porosity and pore density of the smooth obstacle:

The analysis of hydrothermal performance, evaluated using the Performance Evaluation Criterion (PEC) coefficient (Figure 5), reveals contrasting results depending on pore density and porosity parameters. No notable improvement is observed for a density of ω = 30 PPI, while a slight improvement appears with ω = 20 PPI, specifically for porosities of ε = 0.86 and 0.92. For ω = 40 PPI, the improvement remains marginal (~0.18%) at ε = 0.8. The optimal configuration is achieved with ω = 50 PPI and ε = 0.8, demonstrating the highest performance improvement on the order of 1.5%. These results underscore the importance of a precise balance between pore density and porosity to maximize hydrothermal efficiency.

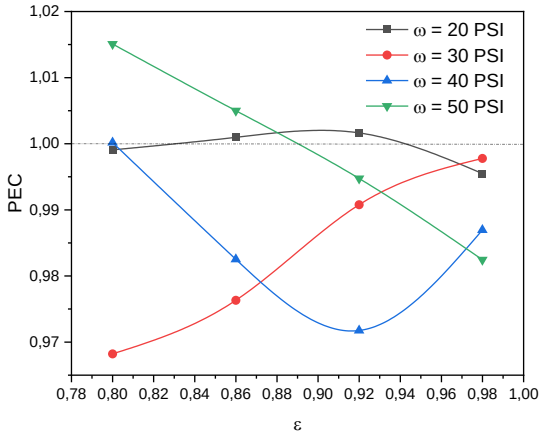

Fig 5: Evolution of the time-averaged PEC for different porosities and pore densities; smooth porous obstacle, H_b=0.5 cm.

c. Effect of the Porous Obstacle's Roughness:

This part of our study examines the influence of the porous cylinder's surface roughness. To model this roughness, we consider surface corrugations for which we will systematically vary two key parameters: the amplitude of the corrugations, which determines the height of the asperities, and the number of corrugations, which characterizes their spatial density. The analysis of Figure 14 reveals that with high porosity (ε = 0.92), modifications to the surface roughness of the porous circular obstacle do not yield any notable improvement in hydrothermal performance. This result indicates that beyond a certain porosity

ISSN: 1737-9334

threshold, the influence of surface microstructure on heat and fluid flow transfer becomes negligible, likely overshadowed by the material's increased permeability. Although this observation suggests the existence of a critical porosity threshold, further investigations are planned to comprehensively confirm this hypothesis.

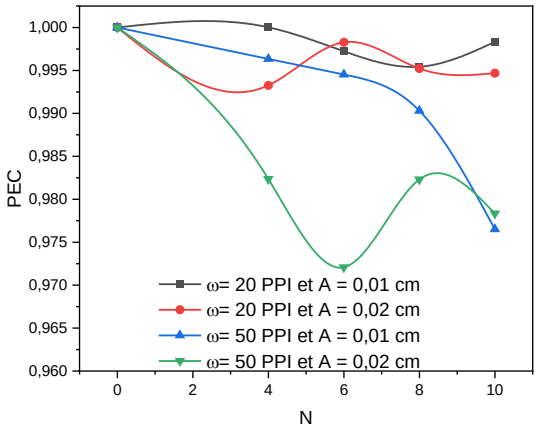

Fig 6: Evolution of the time-averaged PEC for different density-amplitude combinations; rough obstacle with ε=0.92 and H_b=0.5 cm.

V. CONCLUSION :

This work investigated the unsteady, laminar, and incompressible forced convection flow of a nanofluid (MWCNT/water) through a straight channel equipped with a rigid baffle and a porous metal foam obstacle. The domain was divided into two compartments separated by the baffle, with a porous block placed in the first compartment, whose surface could be rough or smooth.

Based on simplifying assumptions, the physical phenomenon was modeled using the Navier-Stokes equations generalized by the Darcy-Brinkman-Forchheimer model, coupled with the energy equation. The resulting system of equations, along with its boundary conditions, was solved numerically using the finite element method.

This study demonstrated the determining influence of three key parameters on the hydrothermal performance of the nanofluid flow around the porous obstacle. The analysis reveals that the optimal baffle height is **H_b = 0.75 cm**, producing the most significant thermal enhancement with a notable increase in the Nusselt number, although it simultaneously generates the highest-pressure losses and induces a transition to a chaotic flow regime. Regarding the porous material properties, the configuration **ω = 50 PPI / ε = 0.8** yields the best performance improvement with a **PEC of +1.5%**, whereas low pore densities (**ω = 20-30 PPI**) show only minimal improvements below **0.5%**. Notably, the study establishes that beyond a porosity of **ε = 0.92**, surface roughness modifications provide no notable improvement, as their influence becomes negligible compared to the material's increased permeability. The identified optimal configuration therefore combines a **H_b = 0.5 cm** baffle for an optimal stability-performance compromise, a pore density of **ω = 50 PPI** with a porosity of **ε = 0.8** to maximize the PEC, and a smooth surface since roughness is only justified at low porosities. These results provide a solid foundation for the design of advanced cooling systems, with quantified performance improvements ranging from **0.18% to 1.5%** depending on the configurations studied.

References:

[1] Amrit Pal Singh Bhinder, Sandip Sarkar, Amaresh Dalal. Flow over and forced convection heat transfer around a semi-circular cylinder at incidence. International Journal of Heat and Mass Transfer 55 (2012) 5171–5184. http //dx.doi.org/10.1016/j.ijheatmasstransfer.2012.05.018

ISSN: 1737-9334

Proceedings of Engineering & Technology -PET Vol 96, pp.95-103 **Advances in Energy Transition and Environmental Impacts**

[2] R. Deepak Selvakumar, S. Dhinakaran. Nanofluid flow and heat transfer around a circular cylinder: A study on effects of uncertainties in effective properties. Journal of Molecular Liquids 223 (2016) 572–588. http://dx.doi.org/10.1016/j.molliq.2016.08.047

[3] Fatih Selimefendigil , Hakan F. Öztop. Magnetic field effects on the forced convection of CuO-water nanofluid flow in a channel with circular cylinders and thermal predictions using ANFIS. International Journal of Mechanical Sciences 146–147 (2018) 9–24. https://doi.org/10.1016/j.ijmecsci.2018.07.011

[4] Amin Nikelham, Vali Enjilela, Nima Vaziri, Zahra Poolaei Moziraji. The effects of magnetic-field direction and magnitude on forced convection of aluminum oxide–water nanofluid over a circular cylinder. International Journal of Thermal Sciences 173 (2022) 107398. https://doi.org/10.1016/j.ijthermalsci.2021.107398

[5] Jing, D., & Zhan, X. Numerical studies on the hydraulic and mixing performances of fluid flow around a cylinder in microchannel with vertical flexible flag. Chemical Engineering Journal (Lausanne, Switzerland: 1996), 430(133009), 133009. doi:10.1016/j.cej.2021.133009

[6] Dadvand, A., Hosseini, S., Aghebatandish, S., & Khoo, B. C. Enhancement of heat and mass transfer in a microchannel via passive oscillation of a flexible vortex generator. Chemical Engineering Science, 207, 556–580. doi:10.1016/j.ces.2019.06.045

[7] Huahai Zhang, Shaotong Fu, Jingxi Dou, Weite Su, Limin Wang. Lattice boltzmann simulation of power-law fluids flow around a forced-oscillation circular cylinder. Computers and Fluids 277 (2024) 106269. https://doi.org/10.1016/j.compfluid.2024.106269

[8] Shohre Heydari , Yasser Amini, Marzie Babaie Rabiee. Convection heat transfer and fluid flow around a circular cylinder with n annular porous coating using the local thermal non-equilibrium model. International Communications in Heat and Mass Transfer 167 (2025)109235https://doi.org/10.1016/j.icheatmasstransfer.2025.109235

[9] Abu-Nada, E.; Chamkha, A.J. Mixed convection flow in a lid-driven inclined square enclosure filled with a nanofluid. Eur. J. Mech. B Fluids 2010, 29, 472–482.

51. Basak, T.; Roy, S.; Pop, I. Heat flow analysis for natural convection within trapezoidal enclosures based on heatline concept. Int. J. Heat Mass Transf. 2009, 52, 2471–2483.

[10] Brinkman, H. The viscosity of concentrated suspensions and solutions. J. Chem. Phys. 1952, 20, 571–581.

[11] Calmidi VV, Mahajan RL. Forced convection in high porosity metal foams. ASME Transactions e Journal of Heat Transfer 2000; 122:557e65.

[12] Boomsma K, Poulikakos D. On the effective thermal conductivity of a threedimensionally structured fluid-saturated metal foam. International Journal of Heat and Mass Transfer 2001;44:827e36.

[13] Sajjad Bouzari, Jafar Ghazanfarian. Unsteady forced convection over cylinder with radial fins in cross flow. Applied Thermal Engineering 112 (2017) 214–225. http://dx.doi.org/10.1016/j.applthermaleng.2016.10.052

ISSN: 1737-9334